The International Journal of Advanced Manufacturing Technology (2019) 101:1821–1835
https://doi.org/10.1007/s00170-018-3029-z

ORIGINAL ARTICLE

Investigation on wear modes and mechanisms of abrasive belts in grinding of U71Mn steel

Zhe He [1,3] · Jianyong Li [1,2] · Yueming Liu [1,2] · Jiwang Yan [3]

Received: 5 August 2018 / Accepted: 12 November 2018 / Published online: 26 November 2018
© Springer-Verlag London Ltd., part of Springer Nature 2018

Abstract
We investigated the wear modes and mechanisms of alumina grits during abrasive belt grinding of U71Mn steel under various normal forces and grinding speeds. Our approach consisted of an experimental procedure that produced sufficient wear followed by a resin-embedding method for observing the cross sections and topographies of grits. Statistics of wear modes and protrusion heights were calculated to visualize and quantify abrasive belt wear. The results demonstrated that different subsurface structures emerged inside the worn grits, and these structures were sensitive to process parameters. Transitions between abrasion and fracture wear modes were frequently observed. The effects of abrasive belt wear and process parameters on wear modes were clarified. The critical protrusion height of the abrasive belts for each wear mode of abrasive grits was experimentally determined.

Keywords Abrasive belt · Wear modes · Wear mechanisms · Subsurface structure

1 Introduction

Abrasive machining is a group of manufacturing methods that employ very hard granular grits to modify the shape and grind the surface texture of manufactured parts. Among various abrasive machining methods, abrasive belt machining has been extensively studied in terms of ground surface [1, 2], particle texture [3], material removal rates [4, 5], contact states [6], power consumption [7], and other factors over the last several years. Like any other cutting tool in the manufacturing process, abrasive belts will inevitably become blunt as the grits planted on the abrasive belt surface slide against the workpiece. Generally, wear impairs the abrasive belt performance and alters the grit geometry, which is detrimental to manufacturing precision and ultimately renders the grinding completely ineffective. However, the effects brought by wear do not always have a negative influence. One example is that wear can renew blunt grits under certain conditions [8].

Previous research on wear modes of abrasive tools mainly focuses on observing the top surface of abrasive tools. Nadolny et al. [9, 10], for example, performed a series of internal cylindrical grinding experiments with grinding wheels. By observing the grits' characteristics, they classified all the grit wear modes into three categories: fracture wear, abrasive wear, and thermo-fatigue wear. In contrast, Liang et al. and Wang et al. [11, 12] thought wear flat, microfracture, grain pull-out, and wheel loading were the four main wear categories during the grinding process. However, some researchers found that there might be subsurface structures beneath the friction surface. Mayer et al. [13] found a layered subsurface structure beneath the ceramic-steel tribology pairs. Klocke et al. [14] found two distinct layers when researching the wear characteristics of sol-gel-corundum grinding with bearing steel. Ding et al. [15] reported subsurface structure between cubic boron nitride (CBN) and metallic materials tribological pair, and such delamination contained different

✉ Zhe He
hezhe_essay@163.com

Jianyong Li
jyli@bjtu.edu.cn

Yueming Liu
liuym@bjtu.edu.cn

Jiwang Yan
yan@mech.keio.ac.jp

[1] School of Mechanical, Electronic and Control Engineering, Beijing Jiaotong University, Beijing 100044, China

[2] Key Laboratory of Vehicle Advanced Manufacturing, Measuring and Control Technology, Ministry of Education, Beijing 100044, China

[3] Department of Mechanical Engineering, Faculty of Science and Technology, Keio University, Hiyoshi 3-14-1, Kohoku-ku, Yokohama 223-8522, Japan

elements. Since it is difficult to examine the internal structure of abrasive grits only by surface observation, the previous researches were very limited in revealing the structures beneath the grinding tool surface. A typical method for observing cross sections is using transmission electron microscopy (TEM) to examine the cross-sectional thin films prepared by the focused ion beam (FIB) technique [16, 17]. However, due to the limitation of the ablating depth to dozens of micrometers [18], this method was not suitable to be applied to grits with average diameters of hundreds of micrometers. We also noticed that quantifying wear modes is an effective way to evaluate the wear of abrasive belts. A few studies have quantified the wear mechanisms of diamond wheels [19]. Unfortunately, no attempt has yet been made to quantify wear modes combining the influence of protrusion height and full grinding time of abrasive belts.

To solve these problems, our work will focus on the following two aims: (1) revealing the wear mechanisms of abrasive belts in the cross-sectional direction by applying the abrasive belt embedding method and (2) investigating the proportion of each wear mode throughout the whole lifecycle of abrasive belts and figuring out the influence of protrusion height on wear modes quantitatively.

Our research topic originates from the rail grinding industry. Thus, the choice of workpiece material and grinding mode are in accordance with actual working conditions. This study was conducted in the following three steps. The first step started with several abrasive belt grinding experiments under different process parameters. Necessary data was collected for further quantitative analysis. The second step presented the wear morphology of abrasive belts including global topographies of abrasive belts and local cross sections of single grit, by applying a resin-embedding method for sample cross sectioning. The third step dealt with the quantitative analysis of each wear mode based on experimental data with different process parameters. This research is expected to provide a comprehensive understanding of wear mechanisms in abrasive belt grinding, which is essential for improving the abrasive belt service life and facilitating the formulation of grinding strategies in rail grinding.

2 Experimental procedure

Strips of U71Mn steel after hot-coiling into a ring were used as the workpieces. This material is the same as the material used in rail grinding industry. In addition, rail grinding was always performed under dry grinding. So, no coolant was involved in our experiments. The chemical compositions of U71Mn are summarized in Table 1. After normalizing, the microstructure of steel was mainly pearlite. Workpiece surface hardness was around 23.3 HRC, and the surface roughness (Ra) was less than 10 μm.

Table 1 Chemical compositions of U71Mn (wt%)

Element	C	Si	Mn	P	S	V	Fe
Percentage	0.75	0.22	1.29	0.016	0.017	0.004	Balanced

Three of the same commercially available abrasive belts were used to test different process parameters in the most repeatable manner possible. Their basic properties are summarized in Table 2. The hardness of abrasive alumina was 60–70 HRC. The average diameter of grits sized 36# was 0.42 mm according to the equation: $d = 15.2\ M^{-1}$, where d is the average diameter and M is the mesh size. Here, we referred to Mei's literature [20] in which the author assumed that the grits were double-ended cones the lengths of which were about three times the average diameter. Thus, the average grit length was $0.42 \times 3 = 1.26$ mm. The embedding depth was nearly half of the grit length, so the average initial protrusion height was about 0.66 mm. Coated density (cm^{-2}) in this study refers to the number of abrasive grits that participate in grinding in one square centimeter.

Experiments under different process parameters were performed based on the abrasive belt grinding apparatus shown in Fig. 1. Motor A drove the driving wheel to force the abrasive belt to rotate at a high velocity, while motor B drove the circular workpiece. The cylinder pushed the abrasive belt to contact the workpiece for grinding. During the grinding process, all the process parameters were controlled by a control box and monitored by a multisensory setup that gathered measurement data in real time. The abrasive belt velocity was monitored by a velocity sensor. An encoder ran synchronously with the workpiece to collect accurate velocity data, and a force sensor was fixed to the contact wheel to collect force data from the cylinder.

The initial workpiece temperature was taken as the ambient temperature, 25 °C. The workpiece moved at a constant velocity of 1 m/s. Three experiments with three same-batch abrasive belts were performed. Each abrasive belt ground the U71Mn specimens for about 20 min under constant normal force and abrasive belt velocity. According to our pre-experiments, a normal force of 350 N and a grinding speed of 37 m/s are the most effective grinding conditions for material removal, so we picked two levels of parameters around the optimum, as shown in Table 3. The experiments were interrupted at regular intervals to take the abrasive belts' surface photos with a digital microscope (1 μm accuracy) to observe the abrasive belts' wear.

A Nanovea PS50 optical profilometer equipped with a white light chromatic sensor (made by Micro Photonics, Inc.) was used to scan the protrusion height distribution of the abrasive belts. It provided the scanning system a vertical measurement range of 3 mm (z direction), a depth resolution of 25 nm, a depth accuracy of 200 nm, a maximum planer

Table 2 Basic items of abrasive belt

Items	Value	Items	Value
Grit size	36	Dimension (m)	3 × 0.075
Average grit size (mm)	1.26	Average initial protrusion height (mm)	0.66
Grit material	Alumina ceramics	Coated density (cm^{-2})	3.8

resolution of 2.6 μm, and a range of sampling rates between 100 and 1000 Hz. At reasonable sample intervals, every point of the surface height was measured to analyze the distribution of protrusion height across the abrasive belts.

A resin-embedding method was used to obtain the cross section of grits. This method is commonly used in the field of biotechnology [21]. Beste et al. [16] thought the cross sections obtained by this method are rather coarse. Since the scale of the grits is very large comparing to typical microstructural features, this shortcoming is not so critical in our cases. The main steps of the resin-embedding method are shown in Fig. 2. Firstly, several small pieces of blunt abrasive belt specimens sized 10 mm × 10 mm were stacked and embedded into hyaline epoxy resin. After the resin solidification, the side surface of each resin-embedded specimen was cautiously polished by sand paper and polishing paste in order to expose the fresh cross section of the grits. To avoid secondary damage during the sample preparation process, the next three rules should be followed: (1) decrease the polishing force and speed slightly, (2) improve the flatness of sample side surface, and (3) avoid the directional scratches on the sample side surface. The cross sections of grits were observed by using microscopes to reveal the wear mechanisms from a new perspective.

3 Results

3.1 Wear morphology

A whole image of the surface topography after grinding operation was taken and shown in Fig. 3. In general, cracks on the abrasive belt surface were the particular characteristic of wear, but several cracks were observed on the brand new abrasive belt surface (Fig. 3(a I)). Such occurrence of cracks was nearly inevitable because the abrasive belts had always been folded tightly in transit. However, the number of cracks increased obviously after grinding due to the repeated mechanical rolling force between workpiece and contact wheel (Fig. 3(II, III, IV)). Most of the cracks expanded in an orientation that was perpendicular to the abrasive belt traveling direction. Four grit behaviors (not involved, abrasion, fracture, and pull-out), shown in Fig. 3(1)–(4), were detected on the abrasive belt surfaces. The four kinds of grit behaviors were frequently observed in the three experiments, but the proportions were different; this will be discussed later.

As shown in Fig. 3(1), many grits coated on the abrasive belt surface were not involved in the grinding process. Such grits almost remained unchanged after grinding. Figure 4 is the cross section of a grit that was not involved in grinding. The grits' (4) summits were sharp and were still able to remove the material. However, the protrusion heights of these grits were so low that all of them were buried under the bonding (2). They did not come into contact with the workpiece or participate in grinding. That is the prime reason why they did not become blunt during grinding. We also observed cracks (3) at the edge of grits in exp. 1 and 3.

Additionally, more than half of the grits cut into the workpiece subsurface and gradually became blunt in shape. The grit wear generally occurred in three forms: abrasion, fracture, and pull-out. Images of these three forms are shown in Figs. 5, 6, 7, 8, 9, 10, and 11, respectively.

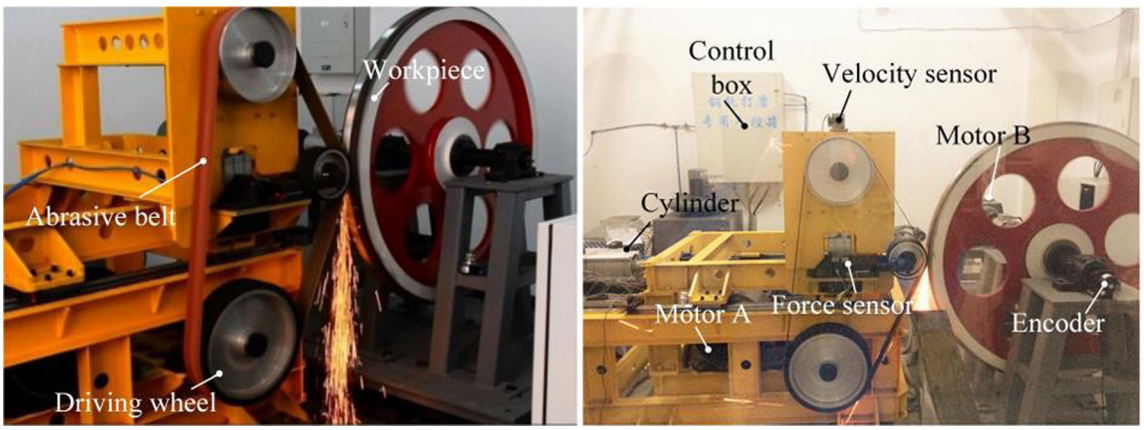

Fig. 1 Abrasive belt grinding apparatus

Table 3 Process parameters of each experiment

Experiment number	Normal force (N)	Grinding speed (m/s)
1	300	30
2	400	45
3	300	45

The SEM image in Fig. 5 depicts facture grit, where a large amount of abrasive debris shed from the grits, creating a random fracture section. After fracture, the grit tip was still sharp and retained moderate cutting ability. The enlarged image of the fracture section (Fig. 4(b)) of the fracture grits shows that the fracture section was not as smooth as an ideal surface. On the contrary, the fracture section was uneven and full of sharp edges, suggesting that the cracks propagated along the grain boundaries due to the relatively weak interfacial strength. Among the grains, tiny pores were spotted, and, very occasionally, some cracks emerged, as shown in Fig. 5(c).

Figure 6 is the cross section of grits that sustained fracture under three sets of different process parameter. In the detailed figure (Fig. 6(d)), many random cracks were observed. Their interconnection eventually caused the grits to break into many small fragments, which is identical to the fracture feature in the SEM image from the top view.

Changing the process parameters had a significant influence on both the number of cracks and the width of cracks. Compared with exp. 3 (Fig. 6(c)), cracks formed in exp. 1 (Fig. 6(a)) were fewer and narrower, which indicated that grinding under higher speed obviously caused more and wider cracks inside the grits. Similar results were detected by comparing exp. 2 (Fig. 6(b)) and 3 (Fig. 6(c)). When the normal force increased, more and wider cracks emerged on the cross sections of grits.

Abrasion (shown in Fig. 7) was another typical wear mode of grits, characterized by a flat, blunt area covered with adhesive materials (U71Mn, as evidenced by EDAX). Grits that suffered abrasion did not readily cut into the workpiece surface if the normal force remained constant—when these blunt grits slid along the surface, the workpiece material was hardly removed. In other words, abrasion significantly weakened the cutting ability of the abrasive belt. From the top view of Fig. 7(b), the blunt area looked uniform and smooth. At higher magnification (Fig. 7(a)), the blunt area was dominated by extremely fine grooves that were nearly identical in pitch and depth. At the edge of the blunt area (Fig. 7(c)), the characteristics under the flat surface were examined in detail: the structure beneath the blunt area consisted of many random particles with diameters around 10 μm. Compared to the smooth surface of the blunt area, these particles disorderly formed a coarse surface, indicating there might be different subsurface structures under the tribological surface, and this point was in accordance with the previous researchers' opinion [13].

To observe the subsurface layered structures under the blunt area, we obtained the cross section by the resin-embedding method. In the meantime, elemental analysis was also conducted in each layer and summarized in Fig. 8. Judging from the obvious structures and elemental differences synthetically, the substructures can be divided into three layers: metal layer, particle layer, and normal layer.

According to Fig. 8, the metal layer mainly consisted of Fe, O, and Mn, but the oxygen content was much higher than that of the workpiece (Table 1). The thickness of this layer was about 5 μm, and it was not uniformly distributed on the blunt area but rather exhibited a generally ribbon-shaped distribution on the topmost part of the blunt area and obviously narrowed along the sliding direction (shown in Fig. 9). With a sensitivity to process parameters, when the grinding speed and normal force increased, the area that the metal layer covered usually decreased (Fig. 9(b)). Additionally, the metal layer gradually moved to the edge of the blunt area (Fig. 9(c)). Some of metal layer were fused with grinding chips, and they dropped from the abrasive belt surface together. Moreover, the metal layer was not tightly adhered on the top of wear grits. It could be easily washed off by an ultrasonic cleaner in our

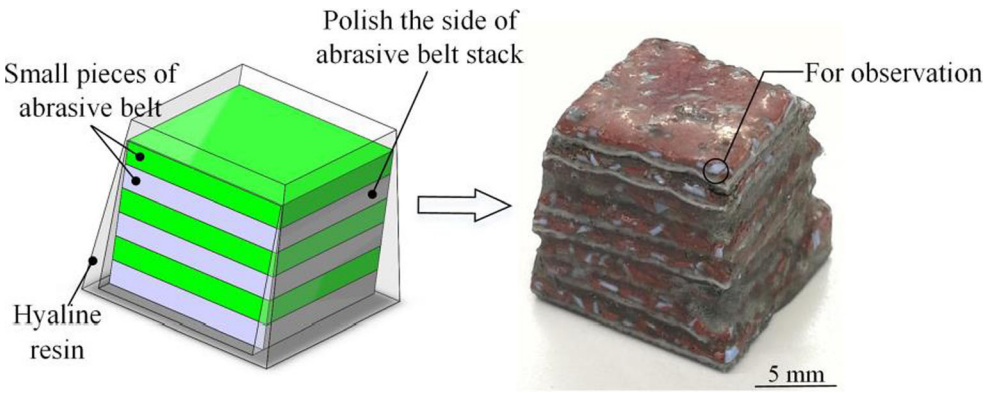

Fig. 2 Resin-embedding method used in abrasive belts wear observation

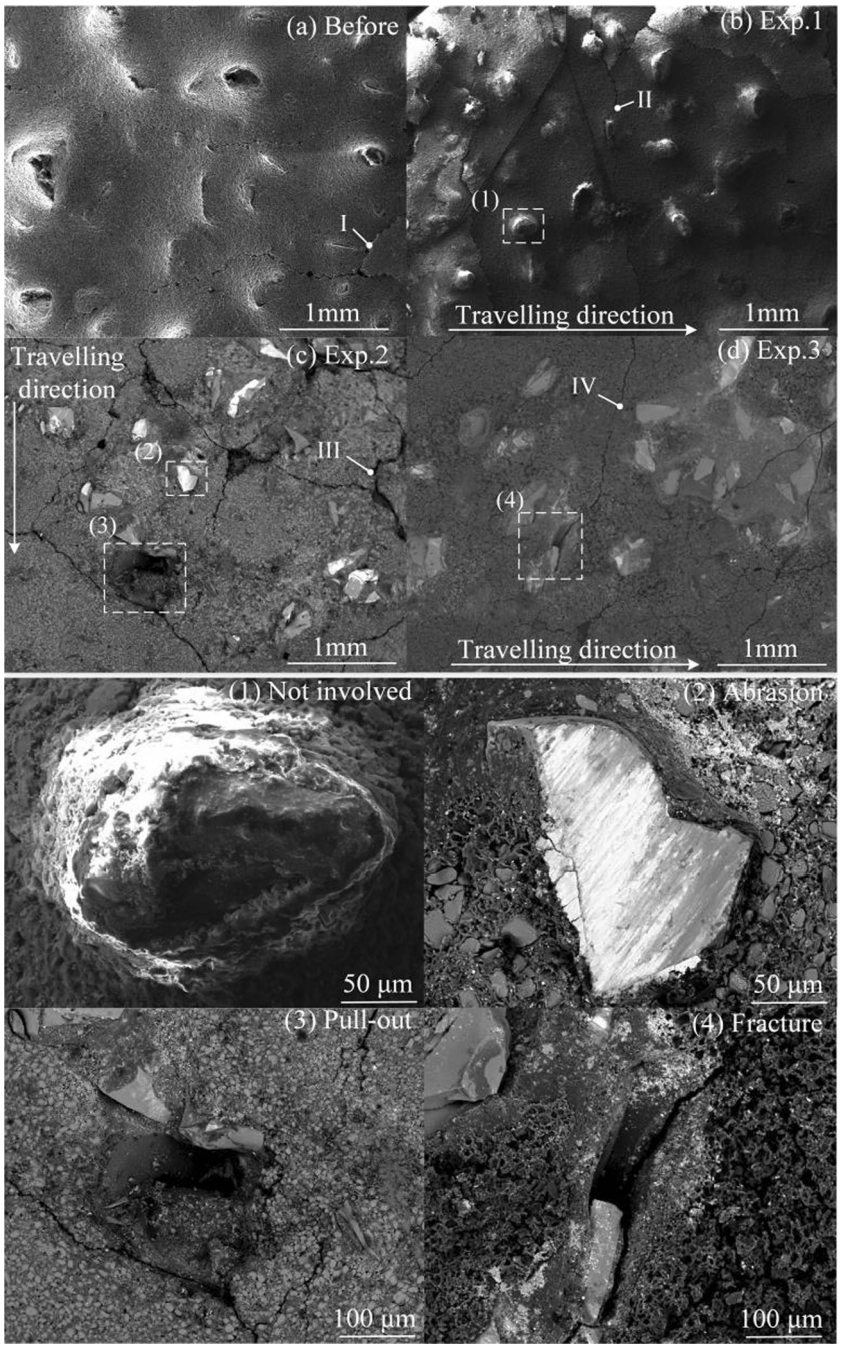

Fig. 3 SEM image of abrasive belt surface before and after grinding and typical grit behaviors (a–d) (1–4)

experiments. Thus, in the grinding process, this layer cannot protect lower layers from continuing wear.

The layer beneath the metal layer was the particle layer (shown in Fig. 10), which mainly contained Al and O. The thickness of this layer varied from 50 to 150 μm. Massive small particles sized around 10 μm and arranged in 5 μm spacing made up this layer. Since the particle size was nearly identical as we saw from the edge of the blunt area in the top view in Fig. 5, the irregular surface of the blunt area was the particle layer. Some alumina fragments (marked with (1) and (4) in Fig. 10(a, c)) were spotted near the particle layer. These might be small fragments dropping from the particle layer.

The related features of this layer were vulnerable to process parameters. When the normal force and grinding speed increased, firstly, the thickness of this layer nearly doubled. Next, the small breaches (marked with (2) in Fig. 10(a)) on the top boundary of the particle layer evolved to long and narrow cracks (marked with (3) in Fig. 10(b)). In the meantime, more and larger fragments (marked with (4) in Fig. 10(c)) dropped from the main part of the grit, causing the top boundary of this layer to become irregular.

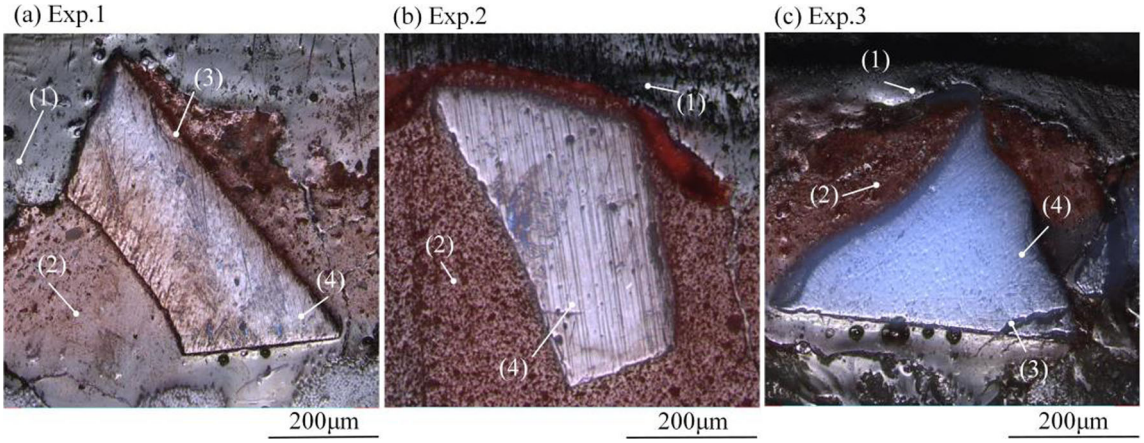

Fig. 4 Cross section of the grit was not involved in grinding (a–c). (1) Hyaline resin, (2) bonding, (3) cracks, and (4) grits

The third layer was the normal layer (Fig. 10). It was located in the deepest position with the largest thickness among the three layers. The element content was almost identical with the particle layer, but the microstructure was completely different: the normal layer consisted of no particles structure but homogeneous and compact component.

Pull-out was the third main mode of abrasive grit wear, in which the entire grit dropped from the abrasive belt without expending any grinding ability and left behind a deep hole on the abrasive belt surface (Fig. 11). In addition, most of the grits that suffered pull-out were concentrated on the periphery of abrasive belt surface cracks. According to their surface topographies shown on the upper corners, the depths of the holes were around 600–700 μm, and there seemed to be no obvious differences among the three process parameters.

3.2 Wear modes transitions

During the grinding process, some grits suffered more than one wear mode. Therefore, some transition patterns between different wear modes must exist. Theoretically, there may have been four transition patterns: abrasion-to-fracture transition pattern, fracture-to-abrasion transition pattern, abrasion-to-pull-out transition pattern, and fracture-to-pull-out transition pattern. According to our statistics, pull-out was quite rare compared with the other two wear modes. So, among all the transition wear patterns, the abrasion-to-fracture transition pattern and the fracture-to-abrasion transition pattern were the two most commonly observed during grinding.

The grits in Fig. 12 were in the stage of abrasion-to-fracture transition pattern. They had the typical feature of abrasion wear—blunt area (3). However, some deep cracks (2) were viewed on the top of the flat, blunt area. Such cracks bridged together, resulting in chunk debris (1) falling from the main part of the grits—the representative characteristic of fracture. When grinding under higher grinding speed and normal force, more cracks emerged on the blunt surface in exp. 2 (Fig. 12(b)) and exp. 3 (Fig. 12(c)) compared with exp. 1 (Fig. 12(a)). Thus, it seems that the transition from abrasion to fracture happened more easily under higher grinding speed and normal force.

Grits shown in Fig. 13 were in the stage transitioning from fracture to abrasion. They had the typical features of fracture and abrasion at the same time. A huge fracture section (1) suggested that grit fracture had happened, while, beside the fracture section, a blunt area (2) indicated that the grits were

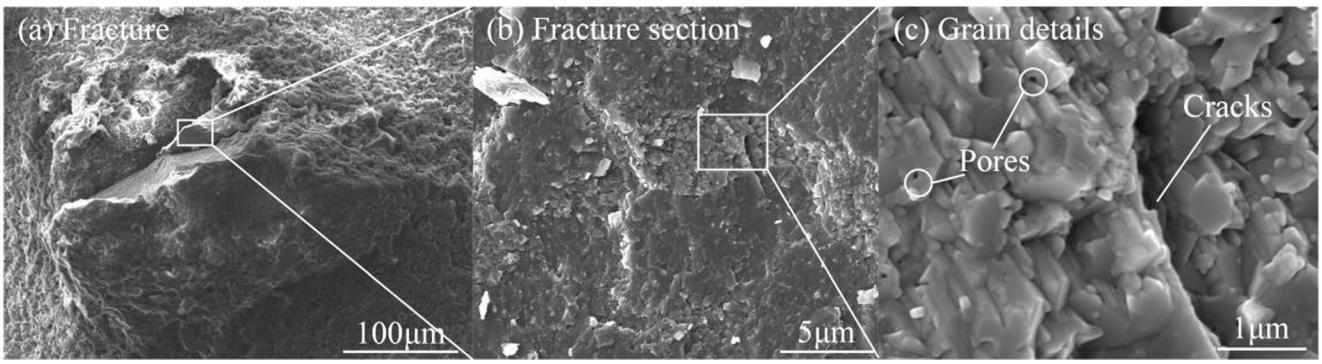

Fig. 5 SEM image of fracture grit and details (a–c)

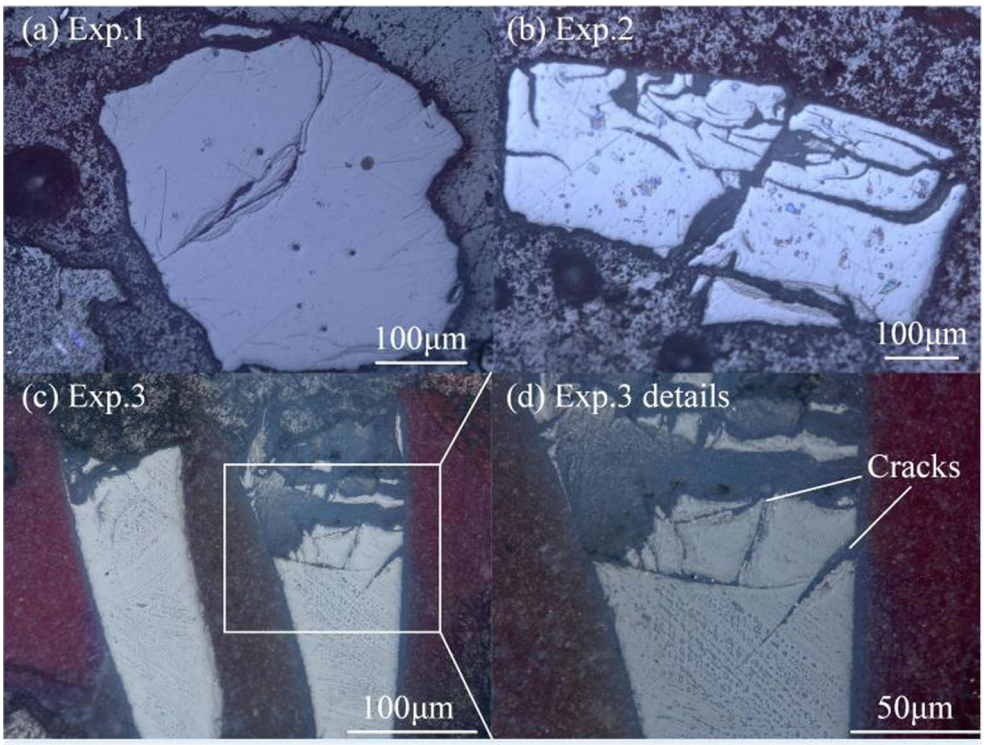

Fig. 6 Cross section of the grits that suffered fracture under different process parameters (a–d)

transforming to the abrasion wear mode. No obvious changes were observed under different process parameters.

3.3 Statistics analysis

3.3.1 Wear mode dependences on process parameters

We calculated some statistics about the proportion of wear modes throughout the whole lifecycle of abrasive belts (Fig. 14). Abrasive belt wear was a random process involving many physical parameters. Thus, the lines of wear mode statistics were slightly fluctuant but did have certain identifiable tendencies across a large time scale. For those grits that suffered more than one wear mode, we only counted the latest wear mode.

As mentioned above, four grit behaviors (abrasion, fracture, pull-out, and not involved) appeared throughout the abrasive belt lifecycle in each experiment. However, as shown in Fig. 14, the proportion of any one behavior differed from the others at various points. Fracture dominated nearly the first 10% of the whole abrasive belt lifecycle, and the peak value of the proportion of grits suffering fracture was around 35%. Grits that sustained abrasion slowly increased in number until becoming the majority after $t = 180$ s. At the end of the abrasive belt lifecycle, the proportion of grits suffering abrasion reached nearly 60% of the total. Pull-out was not the main wear mode at any point in the grinding process: an average of only 8% of the grits dropped from the abrasive surface without turning blunt. The pull-out phenomenon slightly alleviated after the first 10% of the whole lifecycle. Not all the

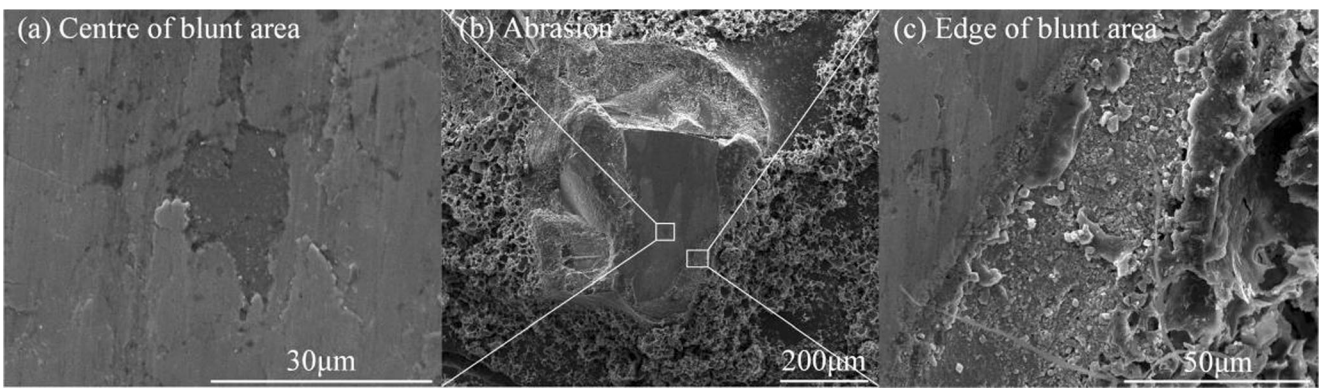

Fig. 7 SEM images of abrasion grit and detailed image (a–c)

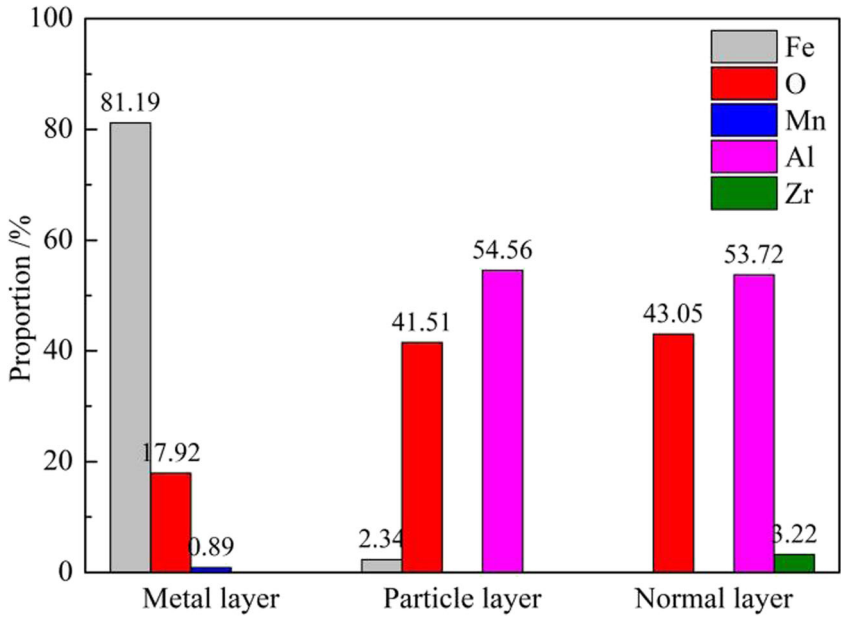

Fig. 8 Element analysis of subsurface layers

grits coated on the abrasive belt surface were involved in grinding. At least 40% of the grits were not involved in grinding even after 20 min of abrasive belt operation, but this percentage decreased as grinding progressed. Zhang et al. [22, 23] reported that nearly 50% of total grits were active in a wheel grinding process, which was smaller compared to our results. The difference between our results may be attributable to variations in contact conditions. A contact wheel covered with an elastic rubber layer was used in our experiments to bear the normal load, creating elastic contact conditions for the abrasive belt grinding process. It was quite different with Zhang et al.'s grinding wheel experiments results, where the contact conditions were assumed to be rigid [24]. An elastic contact allowed more grits with lower protrusion height to come into contact with the workpiece, so the percentage of not-involved grits was smaller than that under a grinding wheel. To some extent, an elastic contact may protect the workpiece surface from secondary damage and cause more cutting grits to be involved in grinding, resulting in a higher material removal rate, which were considered to be the two main advantages for abrasive belt grinding [25].

The effects of process parameters on each wear mode were also analyzed. Two different levels of normal force and grinding speed were adjusted to conduct three experiments. By comparing exp. 1 and 3 in Fig. 14(b, c), we found that fracture and pull-out became more frequent at higher grinding speeds. A higher normal force also led to a higher incidence of fracture and pull-out, which was determined by comparing exp. 2 and 3 in Fig. 14(b, c). The latter result was consistent with the study reported by Wang et al. [8].

3.3.2 Wear modes dependence on grit protrusion height

During the experiments, we also noticed that the protrusion height of the abrasive belt profoundly influenced the wear modes due to the protrusion height discrepancy of new and blunt abrasive belts. Therefore, we measured the protrusion height distribution of the abrasive belt in exp. 1 at two points: the beginning and end of grinding, which corresponded to grinding times from 0 to 60 s and 1307 to 1367 s, respectively.

The abrasive belt surface was composed of many calibrated needle-shaped grits that were electrostatically

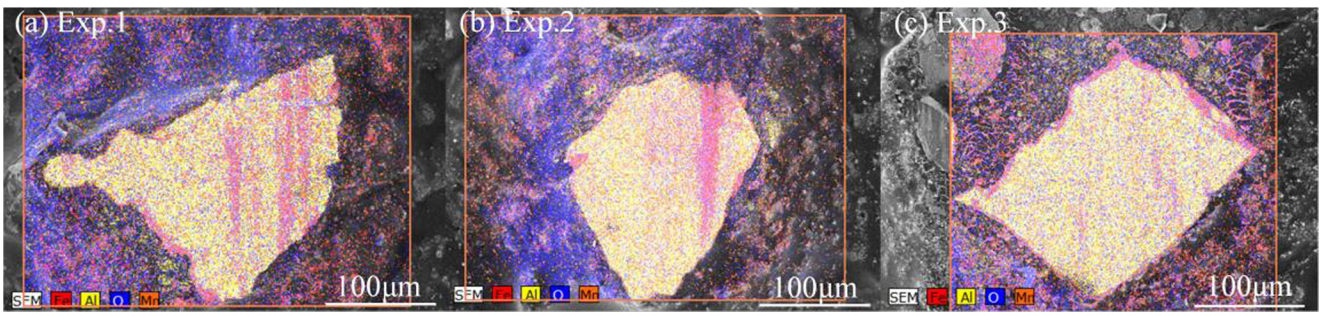

Fig. 9 Metal layer on the top of blunt area (a–c)

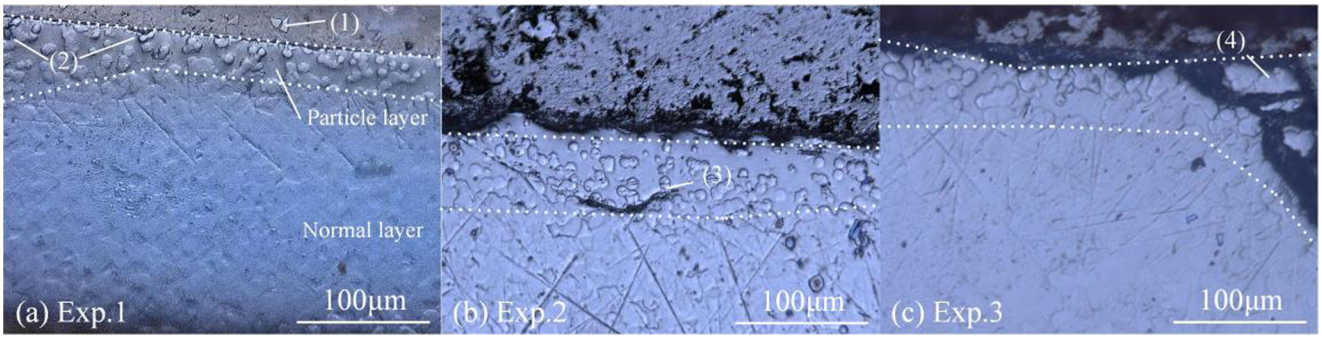

Fig. 10 Cross sections of abrasion grits (a–c). (1) Small fragments, (2) breaches, (3) cracks, and (4) big fragments

deposited on the polyester backing. Due to their random diameters, the protrusion heights of abrasive grits were also random accordingly. By the method provided in literature [26], we collected the protrusion heights of new abrasive belts and blunt abrasive belts in Fig. 15. The mean and standard deviation for new abrasive belts are μ_1 and σ_1, while the mean and standard deviation for blunt abrasive belts are μ_2 and σ_2. The distribution of new abrasive belt protrusion height followed a Gaussian distribution as confirmed by a skewness-kurtosis test. However, after grinding, the distribution of blunt abrasive belt protrusion height no longer matched with a Gaussian distribution, for the standard deviation was extremely small. In other words, the protrusion height of a worn abrasive belt was generally lower than that of a new abrasive belt, but its protrusion height was more uniform. In addition, the worn abrasive belts' protrusion heights above a certain threshold were artificially removed, creating a huge difference with new abrasive belts in maximum protrusion height. It should be noted that the protrusion height was not zero although the belts had been ground for more than 20 min, at that time, the material removal rate was nearly lower than one sixth of the initial material removal rate. Considering the time cost of grinding, the abrasive belts should be replaced in a timely manner.

To explore the internal relation between protrusion height and wear modes, statistics were calculated on the proportions of wear modes under different protrusion heights. The protrusion heights of new and blunt abrasive belts were quite different, as confirmed in Fig. 15, so our statistics were determined for both new and blunt abrasive belt.

Figure 16 quantitatively describes the difference of grit behaviors for both the new (grinding time from 0 to 60 s) and worn (grinding time from 1307 to 1367 s) abrasive belts in exp. 1. The new abrasive belt (Fig. 16(a)) grits with higher protrusion heights were likely to sustain fracture, which was the same as what Eiss reported in the literature [27]. The specific protrusion height range for fracture was above $\mu_1+\sigma_1$ (0.9 mm). Grits with protrusion height around the mean value ($\mu_1-\sigma_1$, $\mu_1+\sigma_1$) (0.4 mm, 0.9 mm) mainly suffered abrasion. In contrast, grits with protrusion height lower than $\mu_1-\sigma_1$ (0.4 mm) were not likely to be involved in grinding. The pull-out probability was quite low (maximum of 5.5%); grits higher than 0.83 mm tended to suffer this wear mode.

Wear modes of the blunt abrasive belt were much simpler. As shown in Fig. 16(b), abrasion was the dominant mode of

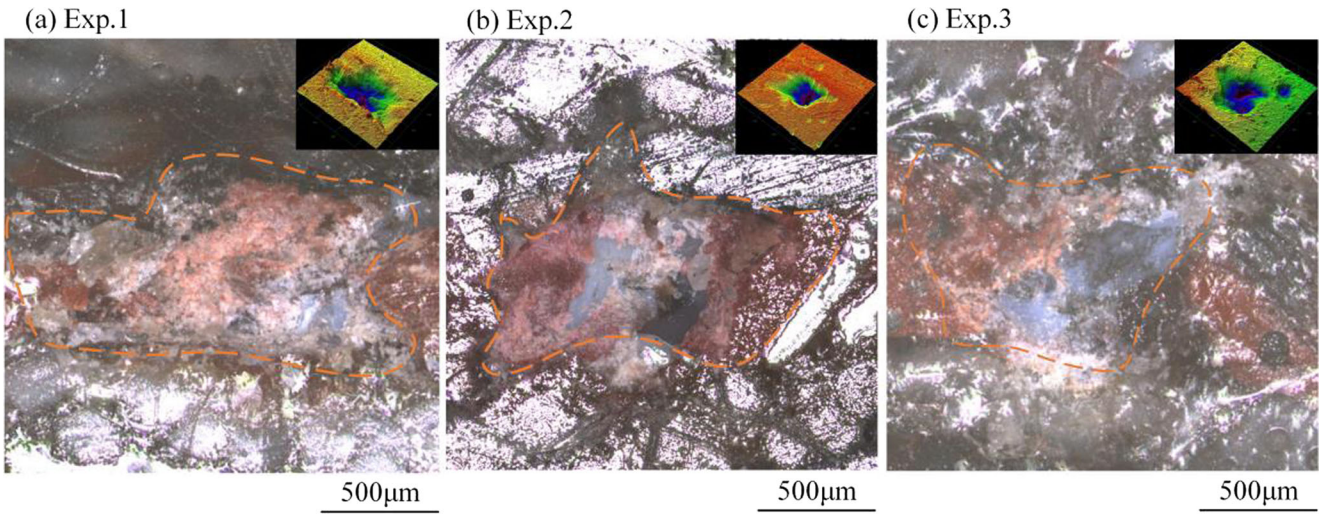

Fig. 11 Cross sections of the grits that suffered pull-out (a–c)

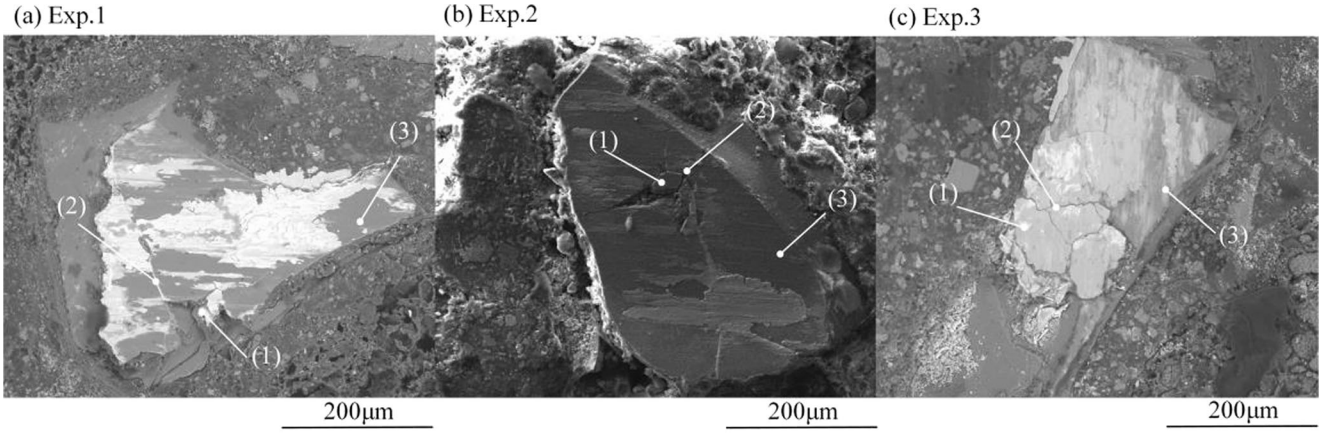

Fig. 12 Wear transition from abrasion to fracture under different process parameters (a–c). (1) Debris, (2) cracks, and (3) blunt area

grit wear under the condition of protrusion heights concentrated from 0.45 to 0.74 mm ($\mu_2-\sigma_2$, $\mu_2+\sigma_2$). Grits lower than 0.45 mm ($\mu_2-\sigma_2$) effectively did not participate in grinding. There were basically no grits with height higher than 0.84 mm, because fracture and pull-out in the early stage of abrasive belt wear practically eliminated those grits.

4 Discussion

4.1 Mechanisms for various wear modes

The protrusion heights of grits that suffered abrasion were generally in the range of $\sigma-\mu$ and $\sigma+\mu$. Abrasion was the main wear mode that impaired the grinding ability. The number of grits that sustained abrasion increased as grinding proceeded but decreased when the normal force and grinding speed were amplified.

Figure 17 illustrates the wear mechanism for abrasion in grinding. Since we abstracted the grits into double-ended cones, the grits that suffered abrasion with the characteristic of blunt area can be roughly simplified as flattop cones. These fragmentary cones consisted of three layers: metal layer, particle layer, and normal layer from top to bottom.

When contact occurred between the grits and the workpiece surface (which formed a tribological pair), the two rough surfaces were, first, subjected to a high level of friction, which led to local heat dissipation at the contact zone [28]. Owing to high pressure and grinding speed, the surface of both materials forming the tribological pair rapidly heated. According to Mayer's work [13], the temperature in the grinding area was around 1500 °C when the mean pulse energy density reached 50 J/mm^2. Once the temperature was higher than the melting point of U71Mn (1370 °C), the workpiece was melted and then oxidized nearly simultaneously. After the liquid phase existed, the local friction coefficient decreased since the tribological pair was sliding under liquid lubrication, so the heat production was reduced in this local area [9]. Liquids then resolidified, leaving the oxides attached on the top of the grit [13, 14]. After the repeated friction between the grits and workpiece, the oxide was daubed into a ribbon shape—metal layer formed.

Grits sliding against the workpiece surface always involved severe deformation and high temperature [18]. The

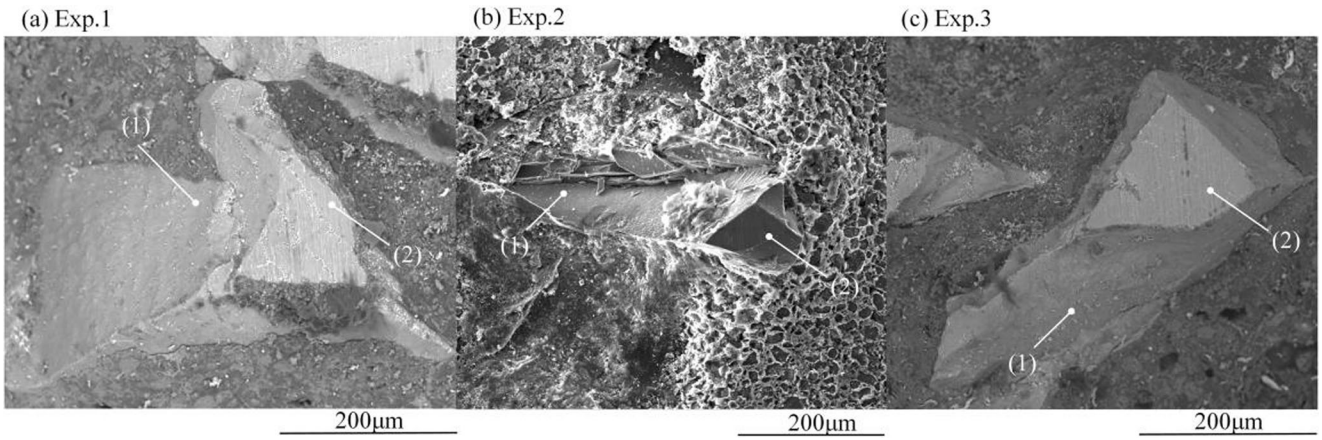

Fig. 13 Wear transition from fracture to abrasion under different process parameters (a–c). (1) Fracture section and (2) blunt area

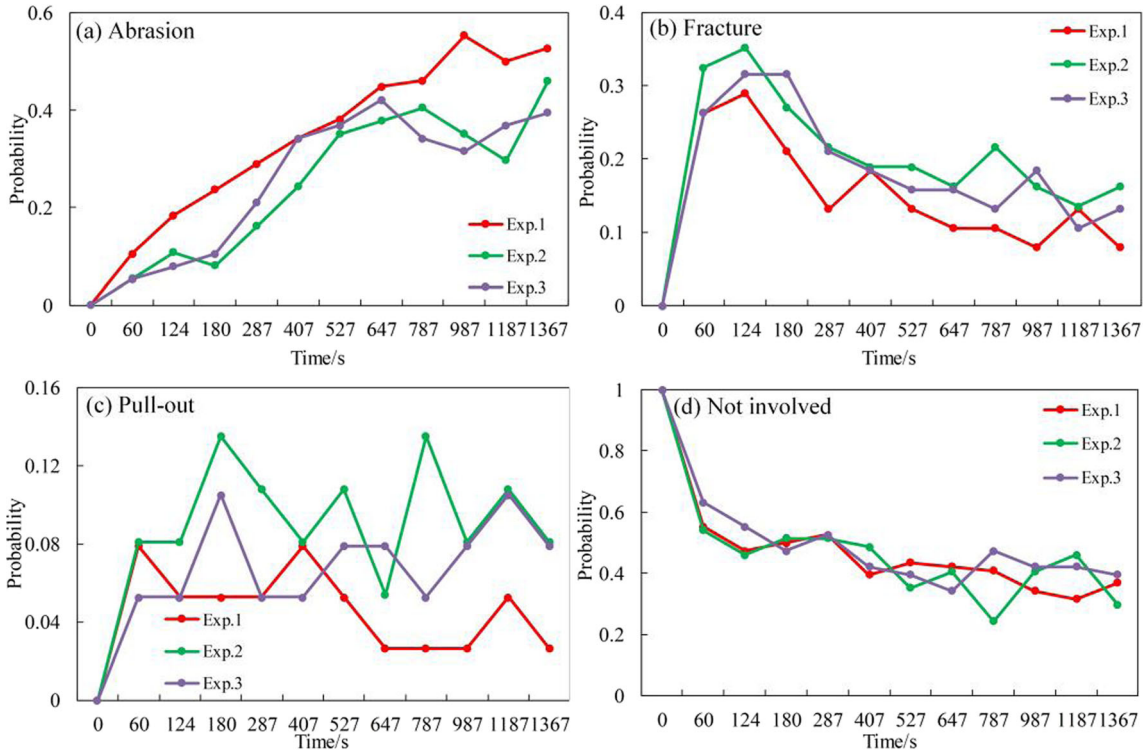

Fig. 14 Different grit behaviors under different process parameters (a–d)

alumina ceramic that constituted the grits was a typical brittle material. Small cracks inside the particle layer emerged due to plastic deformation on the top of the particle layer [16]. Such cracks in the particle layer expended and bridged, causing small fragments to fall off the main part of the grit, indicating the particle layer was consumed continuously. Consequently, the top surface of the particle layer was not smooth [29].

At a certain depth below the surface, the interior of the grits was not influenced by heavy plastic deformation associated with high temperature, nearly no damages were observed, and the material maintained its original structure. Thus, this layer was called normal layer. As the wear proceeded, the particle layer was consumed and became thinner. The influence of plastic deformation and temperature could then reach greater depths, so the normal layer turned into the particle layer and

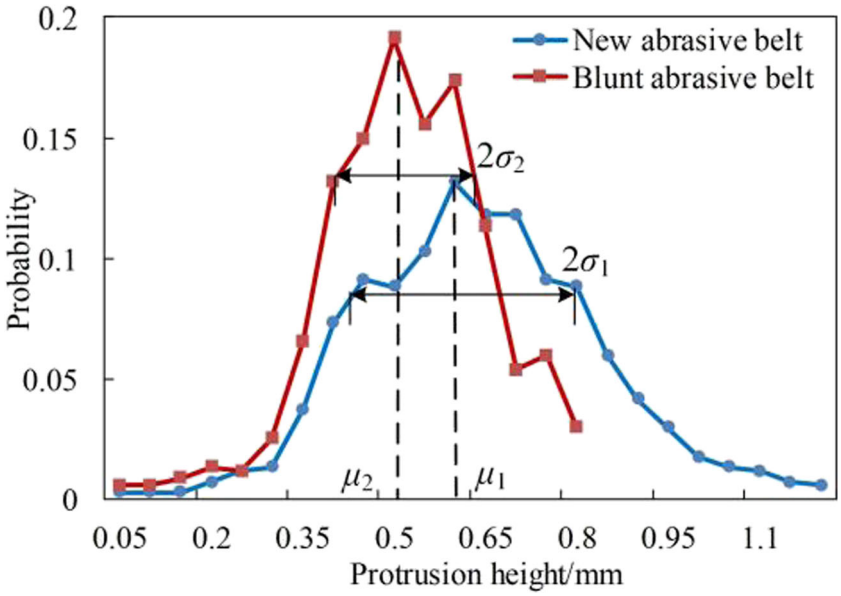

Fig. 15 Distribution of protrusion height before and after grinding in exp. 1

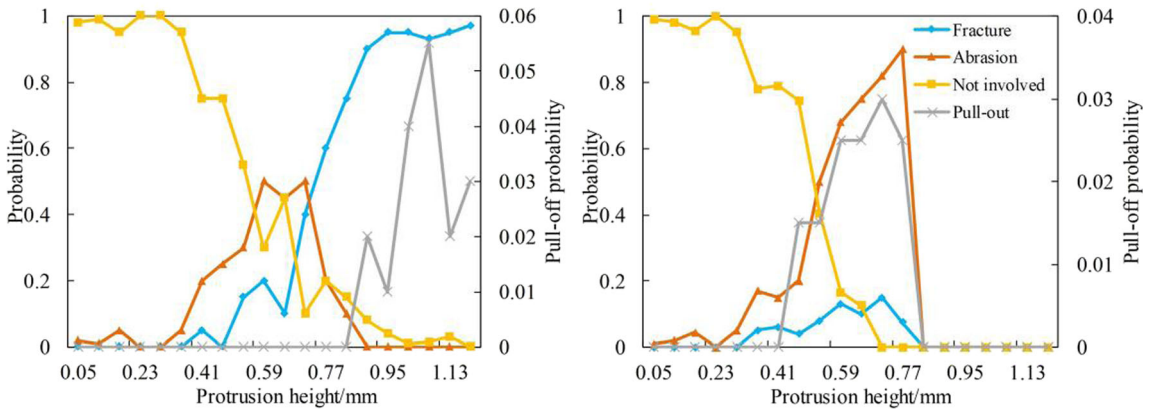

Fig. 16 Wear modes probability for new and worn abrasive belts in exp. 1 (a and b)

was covered by the U71Mn metal layer again. Then, the grit repeated the wear process above.

Naturally, as the normal force and grinding speed increased, the effect of plastic deformation and high temperature was more significant. As a result, the cracks were more frequent. More and larger fragments dropped from the main parts of the grits, which indicates that the grits were consumed much faster than before.

Figure 18 depicts the wear mechanism for fracture. The grits whose protrusion height was higher than $\mu+\sigma$ were vulnerable to fracture. As the grinding process went on, the number of grits that suffered from fracture decreased obviously. Fracture was mainly caused by the initial pores and cracks that were formed in the grit production process. A highly multiaxial stress state formed inside the ceramic grits once the grits participated in grinding. Stress concentration existed near the initial pores and cracks. Since the ceramics was a brittle material with strong resistance to compression but weak resistance to tension [30], the damage emerged in these tensile stress concentration regions. With further loading, new cracks appeared at the edge of initial cracks and pores, they expanded in the most unsubstantial direction—the grain boundaries direction—intergranular fracture occurred [31], as verified in Fig. 5. With additional wear, more cracks formed. These cracks bridged together and even penetrated the grits. Finally, the debris fell from the grits then new fracture section came into being—the signature feature of fracture. Increasing the normal force and grinding speed accelerated the generation and expansion of cracks, which directly increased the number and width of the cracks inside the grits.

Grinding wheels usually consist of multiple layers of grits coated on the surface. Some blunt grits on the top surface will be removed to expose subsequent sharp grits involved in grinding. However, the abrasive belts consist of only one layer of grits. There are no replaceable grits in abrasive belt grinding. Accordingly, pull-out means a negative impact on the grinding ability of abrasive belts. Generally, the mechanism for pull-out involves two aspects: one is low bonding strength between the boundary of grits and resin. The other is low tensile strength inside the resin itself. Researchers [11, 31] thought that when the grinding force was larger than a critical threshold, the bond connecting with neighboring grits may fracture, leading to pull-out. But before the fracture, the deformation of resin may not be noticed by most researchers. Figure 19 illustrates the mechanism of pull-out for resin-bonded grits. Multiple studies [12, 32] reported that the resin is a kind of porous material. Some voids near the grit were distorted into an ellipse as the result of the force borne by the grits. This was called void expansion [33]. As deformation increased, the resin yielded, causing the bridge between two voids to become thinner and break. Consequently, some amount of resin bonding usually adhered to the pull-out grits,

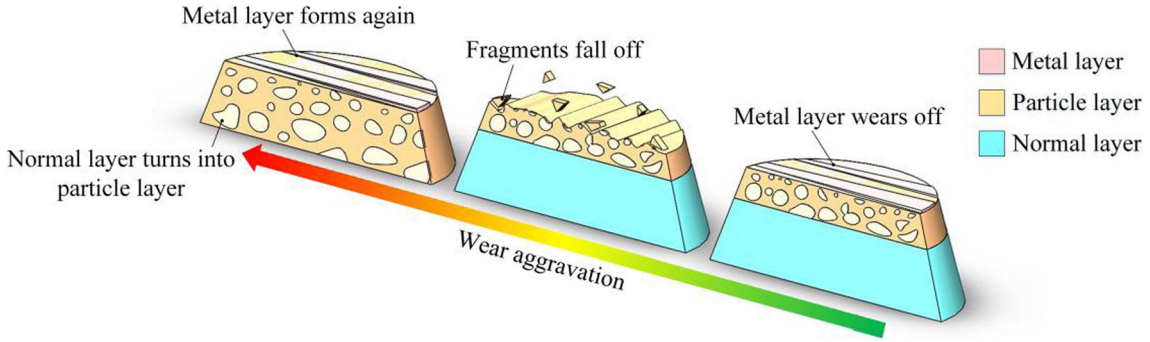

Fig. 17 Wear mechanism for abrasion

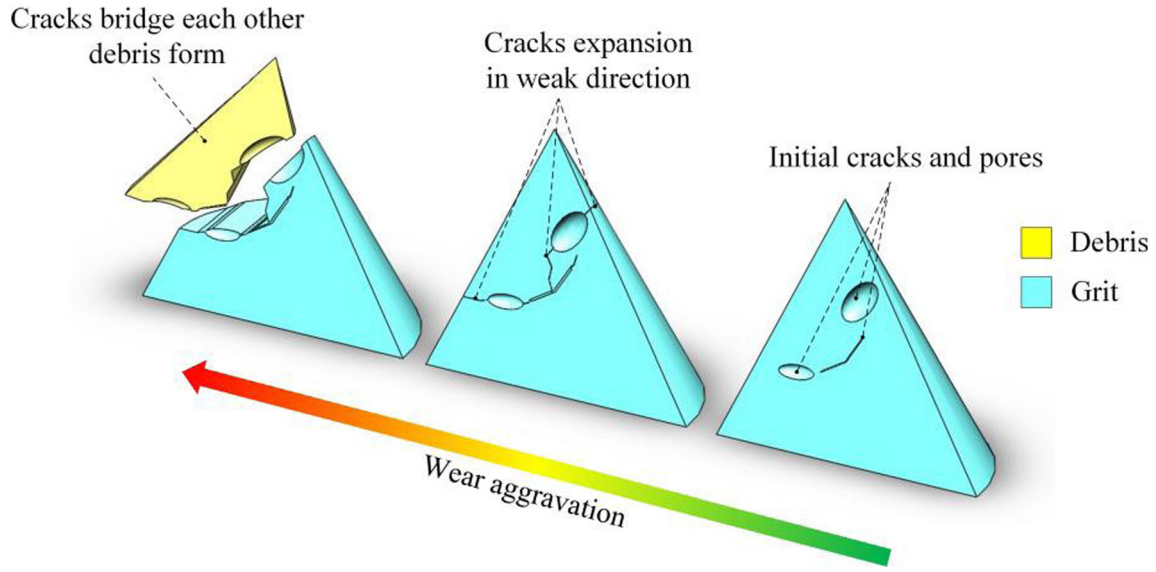

Fig. 18 Wear mechanism for fracture

leaving the pits shaped irregularly. This also explained why grits that suffered pull-out were concentrated near cracks in the surface of the abrasive belt. The bonding force on the interface of grits being lower than the grinding force was also an important reason responsible for pull-out. Higher normal force and grinding speed aggravated the deformation of resin resulting in more grits dropping from the abrasive surface.

4.2 Mechanism for wear mode transitions

The protrusion height distribution changed appreciably due to the wear during the abrasive belt lifecycle [34], as evident in Fig. 15. Additionally, a single grit is usually subjected to varied grinding conditions. The changing grinding condition for the single grit should be responsible for transition mechanisms.

Figure 20 illustrates the mechanism for wear transition. For a new abrasive belt, the distribution of protrusion height followed a Gaussian distribution. When the abrasive belt came into contact with the workpiece, only a few grits with the greatest protrusion heights were involved in grinding. However, the situation was quite different for a blunt abrasive belt, whose protrusion height was lower but more uniform, so more grits contacted the workpiece at the same moment. Assuming that the normal force stayed constant during the grinding process, the stress for a single grit on a blunt abrasive belt was much smaller than that of a single grit on a new abrasive belt. Grits borne greater normal force is likely to suffer fracture. Therefore, in the early stage of abrasive belt grinding ($t < 180$ s), the fracture mode predominated. As wear proceeded, the proportion of grits suffering abrasion rose gradually and then

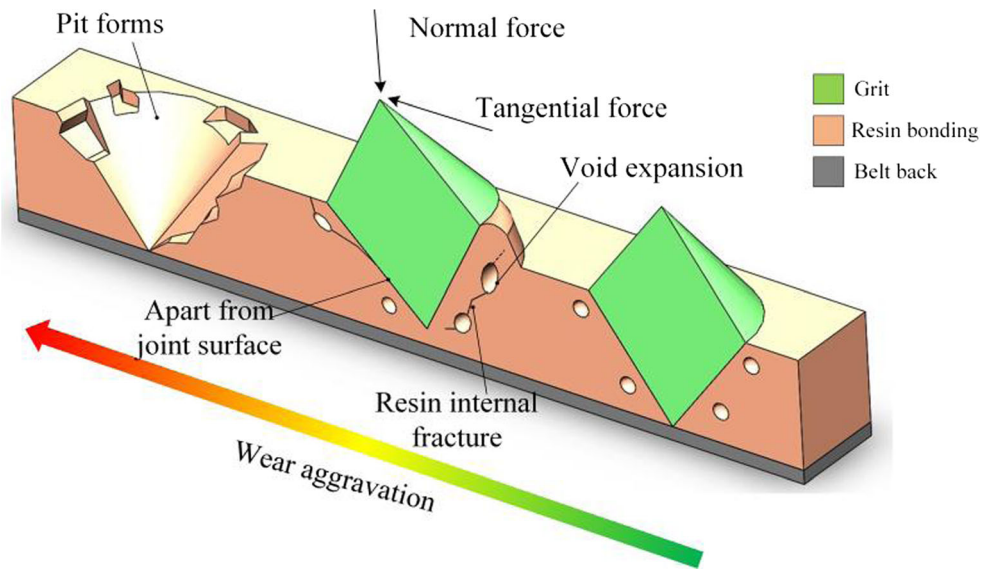

Fig. 19 Wear mechanism for pull-out

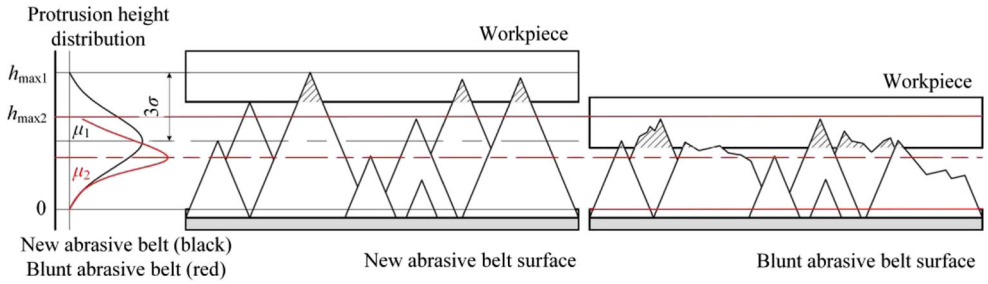

Fig. 20 Mechanism for wear transition

took the majority after $t = 180$ s. When increasing the normal force and grinding speed, the transition between abrasion and fracture was pushed backward, that is, it took more time for the proportion of abrasion to exceed that of fracture.

On a microscale level, if the stress underneath the formed blunt area was greater than a certain threshold, it may cause subsurface cracks to propagate along the grain boundary. Eventually, these cracks connected with each other and opened to the surface. Chunk debris detached from the grit, leading to fracture. Opposite results were obtained when the stress was lower than the threshold. The cracks did not extend any more. Grits that sustained fracture were consumed much more slowly, and abrasion occurred.

According to the above theories, appropriately increasing the speed and normal force of grinding at the late stage may induce the abrasion mode to transform to the fracture mode in order to sharpen the grits and improve the durability of abrasive belts.

5 Conclusions

The wear mechanisms for alumina grits coated on abrasive belts in the steel grinding process were investigated by applying the resin-embedding method to sample cross sectioning. Quantitative analysis was performed to clarify wear regularities along the abrasive belt lifecycle. Conclusions were summarized as follows:

1) Fracture, abrasion, and pull-out were the dominant wear modes in the lifecycle of abrasive belts. In grinding, the proportion of fracture, first, ascended to around 30% and then descended, while the proportion of abrasion rose steadily and exceeded that of fracture after grinding for 180 s. In addition, this time point would be slightly pushed backward under higher grinding speed and normal force. Pull-out showed a very low proportion (< 8%). Nearly 40% of grits were not involved in grinding.
2) Fracture wear featuring with huge fracture section was caused by initial pores and cracks inside the grits. Under multiaxial stress, the cracks extended along grain boundaries and then bridged together, resulting in debris dropping from the main parts of grits. Under higher grinding speed and normal force, the width and number of internal cracks increased. Abrasion was characterized by a smooth blunt area. The subsurface of a blunt area consisted of three layers: metal layer, particle layer, and normal layer from top to bottom. By increasing the normal force and grinding speed, cracks and fragments formed in the particle layer. Pull-out was the result of the low adhesion strength and low tensile strength of the resin bond.
3) The main reason for wear mode transition was the change of the grinding condition for a single grit after wear had occurred. Transition between fracture and abrasion wear modes was significant in the grinding process.
4) The protrusion height of abrasive grits changed from a Gaussian distribution to a uniform distribution due to wear. Grits the protrusion height of which lies in the range of ($\mu-\sigma$, $\mu+\sigma$) were mainly dominated by abrasion. Grits lower than $\mu-\sigma$ were likely not involved in grinding, while grits higher than $\mu+\sigma$ mainly sustained fracture or pull-out.

The future direction of this work will focus on the formation mechanism for the layered structure in abrasion grits.

Funding information The first author of this paper (Zhe He) would like to acknowledge the financial support from "China Scholarship Council (201707090012)" which helped his stay in Japan for international joint research. This paper is supported by "the Fundamental Research Funds for the Central Universities" (2018JBZ105).

Publisher's Note Springer Nature remains neutral with regard to jurisdictional claims in published maps and institutional affiliations.

References

1. Ma GL, Yang JQ, Liu Y, He SY, Jiang ZH (2013) Friction and wear behavior of nanocrystalline nickel in air and vacuum. Tribol Lett 49(3):481–490
2. Pandiyan V, Tjahjowidodo T, Samy MP (2016) In-process surface roughness estimation model for compliant abrasive belt machining process. Procedia CIRP 46:254–257
3. Guo ZW, Yuan CQ, Yan XP, Peng ZX (2014) 3D surface characterizations of wear particles generated from lubricated regular concave cylinder liners. Tribol Lett 55(1):131–142

4. Yun H, Yajie W, Haining L, Yaxiong C, Zhongsheng Y (2015) Application model of surface removal contour to blade abrasive belt grinding. Int J Abrasive technology 7(2):122–136
5. Wang YJ, Huang Y, Chen YX, Yang ZS (2015) Model of an abrasive belt grinding surface removal contour and its application. Int J Adv Manuf Technol 82(9–12):2113–2122
6. Jourani A, Dursapt M, Hamdi H, Rech J, Zahouani H (2005) Effect of the belt grinding on the surface texture: modeling of the contact and abrasive wear. Wear 259(7–12):1137–1143
7. Daniel ES, Richard LL, Steven DJ (2005) Abrasive machining process characterization on matierial removal rate final surface texture and power consumption for wood. For Prod J 55(12):35–41
8. Wang W, Salvatore F, Rech J, Li J (2017) Investigating effects of adhesion wear on cutting efficiency and energy cost in dry belt finishing. Int J Adv Manuf Technol 95(5–8):2119–2123
9. Nadolny K (2014) Wear phenomena of grinding wheels with sol–gel alumina abrasive grains and glass–ceramic vitrified bond during internal cylindrical traverse grinding of 100Cr6 steel. Int J Adv Manuf Technol 77(1–4):83–98
10. Nadolny K, Kapłonek W (2016) The effect of wear phenomena of grinding wheels with sol-gel alumina on chip formation during internal cylindrical plunge grinding of 100Cr6 steel. Int J Adv Manuf Technol 87(1–4):501–517
11. Liang ZQ, Wang XB, Wu YB, Xie LJ, Liu ZB, Zhao WX (2012) An investigation on wear mechanism of resin-bonded diamond wheel in elliptical ultrasonic assisted grinding (EUAG) of monocrystal sapphire. J Mater Process Technol 212(4):868–876
12. Wang Q, Zhao W, Liang Z, Wang X, Zhou T, Wu Y, Jiao L (2018) Investigation of diamond wheel topography in elliptical ultrasonic assisted grinding (EUAG) of monocrystal sapphire using fractal analysis method. Ultrasonics 84:87–95 **Mar**
13. Joachim M, Robert E, Rosemarie B, Thomas W, Cleo H, Fritz K (2006) Wear characteristics of second-phase-reinforced sol–gel corundum abrasives. Acta Mater 54(13):3605–3615
14. Klocke F, Engelhorn R, Mayer J, Weirich T (2002) Micro-analysis of the contact zone of tribologically loaded second-phase reinforced sol-gel-abrasives. CIRP Ann 51(1):245–250
15. Ding W, Linke B, Zhu Y, Li Z, Fu Y, Su H, Xu J (2017) Review on monolayer CBN superabrasive wheels for grinding metallic materials. Chin J Aeronaut 30(1):109–134
16. Ulrik B, Staffan J (2008) Targeting micro-sectioning—a technique to study subsurface features in worn specimens. Wear 264(11–12): 1152–1156
17. Wan L-B, Li S-X, Lu S-Y, Su Y-S, Shu X-D, Huang H-B (2018) Case study: formation of white etching layers in a failed rolling element bearing race. Wear 396-397:126–134
18. Zeng P, Rainforth WM, Stewart TD (2017) Characterisation of the wear mechanisms in retrieved alumina-on-alumina total hip replacements. Wear 376-377:212–222
19. Liao TW, Li K, Mcspadden SB Jr (2000) Wear mechanisms of diamond abrasives during transition and steady stages in creep-feed grinding of structural ceramics. Wear 242:10
20. Mei YM, Yu ZH, Yang ZS (2016) Numerical investigation of the evolution of grit fracture and its impact on cutting performance in single grit grinding. Int J Adv Manuf Technol 89(9–12):3271–3284
21. Mcdonald KL (2014) Rapid embedding methods into epoxy and LR White resins for morphological and immunological analysis of cryofixed biological specimens. Microsc Microanal 20(1):152–163 **Feb**
22. Zhang ZY, Huo YX, Guo DM (2013) A model for nanogrinding based on direct evidence of ground chips of silicon wafers. SCIENCE CHINA Technol Sci 56(9):2099–2108
23. Zhang ZY, Song YX, Xu CG, Guo DM (2012) A novel model for undeformed nanometer chips of soft-brittle HgCdTe films induced by ultrafine diamond grits. Scr Mater 67(2):197–200
24. Zhi SD, Li JY, Zarembski AM (2014) Modelling of dynamic contact length in rail grinding process. Front Mech Eng 9:242–248
25. He Z, Li JY, Liu YM, Nie M, Fan WG (2017) Investigating the effects of contact pressure on rail material abrasive belt grinding performance. Int J Adv Manuf Technol 93(1–4):779–786
26. Blunt L, Ebdon S (1996) The application of three-diensional surface measurement techniques to characterizing grinding wheel topography. Int J Mach Tools Manufact 36(11):1027–1126
27. N. S. Eiss J. (1967) Fracture of abrasive grain in grinding. Journal of Engineering for Industry, 89(3): 463–469
28. Katsuki F (2013) Subsurface characteristics of a Fe–0.4wt%C martenstic steel abraded with nanoindentation and cross-sectional TEM techniques. Wear 303(1–2):92–97
29. Linke BS (2015) Review on grinding tool wear with regard to sustainability. J Manuf Sci Eng 137(6):060801
30. Nadolny K (2014) State of the art in production, properties and applications of the microcrystalline sintered corundum abrasive grains. Int J Adv Manuf Technol 74(9–12):1445–1457
31. Wang ZY, Li PF (2015) Dynamic failure and fracture mechanism in alumina ceramics: experimental observations and finite element modelling. Ceram Int 41(10):12763–12772
32. Liu D, Tsoi JK-H, Pow EH-N, Wong HM (2015) Influence of different etching protocols on the reliability of resin bonding to CAD/CAM feldspathic porcelain. Int J Adhes Adhes 62:18–24
33. Kamiya K, Suzuki N (2016) A low-temperature fast curing latent catalyst microencapsulated in a porous resin structure. Int J Adhes Adhes 68:333–340
34. Godino L, Pombo I, Sanchez JA, Alvarez J (2018) On the development and evolution of wear flats in microcrystalline sintered alumina grinding wheels. J Manuf Process 32:494–505